Al 27 NMR local study of the Al0.5TiZrPdCuNi alloy in high-entropy alloy and metallic glass forms

N.B. When citing this work, cite the original published paper.

(article starts on next page)

^{27}Al NMR local study of the Al$_{0.5}$TiZrPdCuNi alloy in high-entropy alloy and metallic glass forms

Magdalena Wencka,[1,2] Matej Bobnar,[1] Tomaž Apih [1], Qiang Hu,[3] Sheng Guo [4], and Janez Dolinšek [1,5,*]

[1]*Jožef Stefan Institute, Jamova 39, SI-1000 Ljubljana, Slovenia*

[2]*Institute of Molecular Physics, Polish Academy of Sciences, Smoluchowskiego 17, PL-60-179 Poznań, Poland*

[3]*Institute of Applied Physics, Jiangxi Academy of Sciences, Changdong Road 7777, Nanchang 330096, People's Republic of China*

[4]*Industrial and Materials Science, Chalmers University of Technology, SE-41296 Göteborg, Sweden*

[5]*University of Ljubljana, Faculty of Mathematics and Physics, Jadranska 19, SI-1000 Ljubljana, Slovenia*

We report a ^{27}Al nuclear magnetic resonance (NMR) local spectroscopic study of the NMR lineshape and Knight shift of a six-component Al$_{0.5}$TiZrPdCuNi metallic alloy that can be prepared either as a crystalline high-entropy alloy (HEA) or as an amorphous metallic glass (MG) at the same chemical composition. For both structural modifications of the material (HEA and MG), we have determined the distribution of electric-field-gradient (EFG) tensors and the local electronic density of states (DOS) $g(\varepsilon_F)$ at the Fermi level at the position of ^{27}Al nuclei. A theoretical $I = \frac{5}{2}$ quadrupole-perturbed NMR spectrum, pertinent to both cubic HEAs and amorphous MGs, has been derived using the Gaussian isotropic model of the EFG tensor distribution, and excellent fits of the experimental spectra were obtained. The EFG distribution function of the MG state is about twice broader than that of the HEA state, reflecting the existence of a (distorted) crystal lattice in the latter and its absence in the former. The T^2 dependence of the Knight shift indicates that the DOS is changing rapidly with energy within the Fermi level region for both structural modifications. The local DOS at the ^{27}Al sites of the HEA sample is ∼10% larger than that of the MG state, indicating comparable degrees of disorder.

I. INTRODUCTION

A characteristic structural feature of high-entropy alloys (HEAs) is a topologically distorted crystal lattice with an immense chemical disorder of five or more principal elements on the lattice sites [1], creating an enormous number of different local chemical environments. Standard structure-determination techniques like x-ray diffraction (XRD) and elastic neutron scattering are unable to characterize the large manifold of local atomic coordination because they give information on the average crystal structure. The extended x-ray absorption fine structure technique is also unable to fully characterize the huge manifold of local chemical environments because it detects radial distribution of atoms in the first few coordination shells but carries no information on their angular distribution relative to the crystallographic axes. Nuclear magnetic resonance (NMR) is a local spectroscopic technique that can determine both the radial and angular distribution of local atomic coordination via the electric quadrupolar interaction between the electric quadrupole moment of the resonant nucleus (of spin $> \frac{1}{2}$) and the electric-field-gradient (EFG) tensor originating from the nearby electric charges (ionic and electronic). In addition, NMR provides information on the local electronic and magnetic structure at the position of the resonant nuclei via the magnetic hyperfine interaction between the nuclear and the electronic spins. Astonishingly, despite the vast literature on the formation, stability, structure, and physical-mechanical properties of HEAs [1–5], no

local spectroscopic study of HEAs with NMR [or other local technique like nuclear quadrupole resonance (NQR), electron paramagnetic resonance (EPR), Mössbauer spectroscopy, or perturbed γ-γ angular correlations] can be found in the literature at the time of writing. In this paper, we report a ^{27}Al NMR study of the lineshape and Knight shift of a six-component Al$_{0.5}$TiZrPdCuNi metallic alloy that can be prepared either as a HEA or as a metallic glass (MG) at the same chemical composition [6–8]. For both structural modifications of the material (HEA and MG), we have determined the distribution of EFG tensors, which directly reflects the distribution of local chemical environments. This has enabled us to make a comparison of the local structural and chemical disorder between a crystalline HEA and an amorphous MG. In addition, the determination of the Knight shift has allowed comparison of the local electronic density of states (DOS) $g(\varepsilon_F)$ in the Fermi level (ε_F) region at the position of the ^{27}Al nuclei for the HEA and the MG states of the same material.

II. MATERIAL AND METHODS

The Al$_{0.5}$TiZrPdCuNi alloy [6–8] is a rare multicomponent metallic alloy that can be prepared either as a HEA [1] or as a MG [9] at the same chemical composition via different synthesis routes. The alloy is related to the class of high-entropy bulk MGs (HE-BMG) [10–13], with the difference that the glassy state of the Al$_{0.5}$TiZrPdCuNi can be prepared as ribbons that are too thin to be classified as a bulk MG (BMG) but conform to the definition of a MG. The preparation steps for both structural modifications of the material are detailed in the previous publications [6–8]. In

*jani.dolinsek@ijs.si

this paper, we are employing the same samples as used in the recent determination of their bulk physical properties (electrical resistivity, thermoelectric power, thermal conductivity, Hall coefficient, specific heat, and magnetic properties) [6], where a thorough structural characterization by XRD, scanning electron microscopy backscattered-electron imaging, and energy-dispersive x-ray spectroscopy (EDS) composition determination and elemental mapping is also presented. To summarize, the MG sample was a melt-spun ribbon of 20 μm thickness and 1 mm width, with an amorphous structure and homogeneously dispersed elements on the micron scale. Its EDS composition was $Al_7Ti_{21}Zr_{15}Pd_{14}Cu_{22}Ni_{21}$. The HEA sample was an ingot of $1.3\,mm^2$ cross-section, prepared by Cu-mold casting. It was composed of crystallites of several micron dimensions, and its structure consisted of two major phases, a body-centered cubic (bcc) with the unit cell parameter $a = 3.10$ Å that occupies $\sim$70% of the volume of the sample and a cubic, Pd_2TiAl-type phase (Heusler alloy, space group $Fm\bar{3}m$, $a = 6.20$ Å, which is exactly twice the bcc cell edge), occupying $\sim$30% of the volume. The bcc phase of composition $Al_5Ti_{19}Zr_{22}Pd_{18}Cu_{19}Ni_{17}$ is close to a random solid solution due to good solubility of the elements. The cubic Pd_2TiAl-type phase of composition $Al_{14}Ti_{16}Zr_{17}Pd_{21}Cu_{15}Ni_{17}$ is structurally related to the bcc phase. The unit cell of the stoichiometric Pd_2TiAl composition can be viewed as a $2 \times 2 \times 2$ supercell composed of eight bcc cells with a specific chemical ordering, where Al and Ti replace each other alternatively in the corners of the bcc cells, whereas Pd is located in the cell centers (for details, see Ref. [6]). Due to the high solid solubility of the elements, the lattice sites are substitutionally disordered, and the actual composition is quite far from the stoichiometric one. Since the unit cell parameter of the cubic Pd_2TiAl-type phase is exactly twice the bcc unit cell parameter, and in view of the high solid solubility of the elements, the entire HEA lattice can be loosely viewed as a single bcc structure, with a larger part of it chemically disordered in a statistical manner and a smaller part of it partially ordered. Magnetic measurements have shown that both the HEA and the MG samples are nonmagnetic (Ni is in a nonmagnetic state in the electrically conducting medium), exhibiting Pauli spin paramagnetism of the conduction electrons [6].

The ^{27}Al NMR experiments were performed in two magnetic fields, which has enabled us to resolve the electric quadrupole and the magnetic hyperfine interactions due to their different dependence on the external magnetic field. The lower field was $B_0 = 8.926$ T, with the reference Larmor frequency of the $AlCl_3$ aqueous solution $\nu_{AlCl_3} = 99.02225$ MHz (using a home-built NMR spectrometer), whereas the higher field was $B_0 = 11.748$ T, with $\nu_{AlCl_3} = 130.3291$ MHz (using a Bruker AVANCE 500 spectrometer). The spectra are strongly inhomogeneously broadened, extending over a frequency interval of about $\pm$1 MHz around the reference frequency, so that recording of the spectrum was done by a frequency-sweep technique with a typical frequency step of 10–50 kHz. At each step, a spin echo was recorded in the time domain, and one half of it was Fourier transformed. The spectral intensity was then integrated in a narrow frequency interval of $\pm$1 kHz around the center irradiation frequency (<1 frequency step), which corresponded to one point in

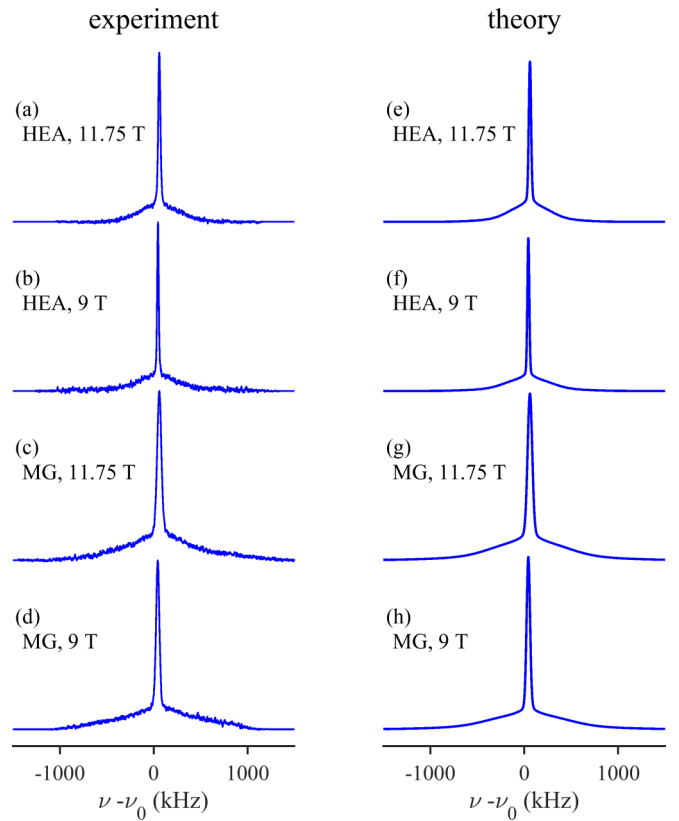FIG. 1. Experimental ^{27}Al nuclear magnetic resonance (NMR) spectra of the $Al_{0.5}TiZrPdCuNi$ high-entropy alloy (HEA) sample at $T = 200$ K in (a) higher magnetic field 11.748 T and (b) lower magnetic field 8.926 T. (c) and (d) Corresponding experimental spectra of the metallic glass (MG) sample. (e)–(h) Theoretical fits of the experimental lineshapes.

the frequency-swept spectrum. At each frequency step, the NMR probehead was tuned automatically via a stepper-motor system. The spectra were recorded at several temperatures between 350 and 80 K. The ^{27}Al lineshape of both investigated samples (HEA and MG) did not change noticeably with the temperature, whereas their center of gravity was temperature dependent, to be discussed in the following.

III. RESULTS AND THEORETICAL ANALYSIS

The experimental ^{27}Al (spin $I = \frac{5}{2}$) frequency-swept spectra of the HEA sample at $T = 200$ K in the higher and lower magnetic fields are shown in Figs. 1(a) and 1(b), whereas the corresponding spectra of the MG sample are shown in Figs. 1(c) and 1(d). The spectra consist of a narrow, high-intensity central line (the $\frac{1}{2} \leftrightarrow -\frac{1}{2}$ spin transition) that is quadrupole-perturbed in the second order and a broad satellite background intensity (the $\pm\frac{1}{2} \leftrightarrow \pm\frac{3}{2}$ and $\pm\frac{3}{2} \leftrightarrow \pm\frac{5}{2}$ transitions), quadrupole-perturbed in the first order. The central lines of the HEA and MG samples in two magnetic fields are shown on an expanded frequency scale in Figs. 2(a) and 2(b), respectively. The second-order quadrupole shift of the central transition is inversely proportional to the external field, whereas the satellites are independent of the magnetic field. All spin transitions are equally shifted by the magnetic hyper-
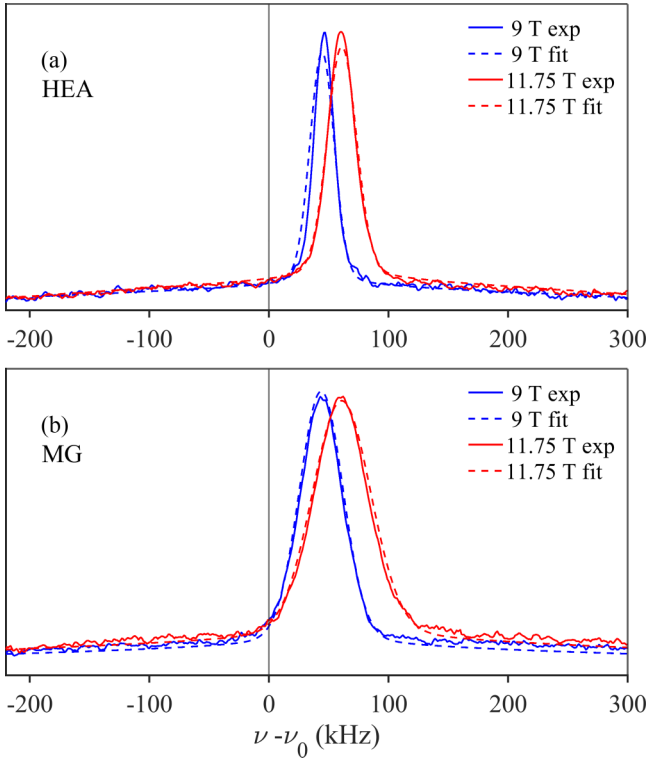
FIG. 2. (a) Experimental central lines of the high-entropy alloy (HEA) sample in two magnetic fields together with the theoretical fits by zooming the spectra from Fig. 1 around the origin. (b) The corresponding experimental and theoretical central lines of the metallic glass (MG) sample.

fine interaction (the Knight shift), with the shift being positive and linear with the field. The Knight shift could be determined on the central line because, on the satellites, it is masked by the much stronger first-order quadrupole interaction. The total shift of the central transition can be written as $\nu - \nu_{\text{AlCl}_3} = \Delta\nu = a/B_0 + bB_0$. Knowing $\Delta\nu$ in two magnetic fields allows the determination of the coefficients a and b that are

associated with the second-order quadrupolar and magnetic shift, respectively. For the HEA sample with $\Delta\nu = 45.1$ kHz in $B_0 = 8.926$ T and $\Delta\nu = 61.2$ kHz in $B_0 = 11.748$ T, we get $a = -31.2$ kHzT and $b = 5.44$ kHz/T, yielding the relative magnetic shift (the Knight shift) at $T = 200$ K $K_{\text{HEA}} = bB_0/\nu_{\text{AlCl}_3} = 4.9 \times 10^{-4}$. For the MG sample, the shifts are $\Delta\nu = 43.5$ kHz in $B_0 = 8.926$ T and $\Delta\nu = 57.7$ kHz in $B_0 = 11.748$ T, yielding $a = -9.0$ kHzT, $b = 5.0$ kHz/T, and $K_{\text{MG}} = 4.5 \times 10^{-4}$ (~10% smaller than K_{HEA}). For comparison, the Knight shift of the bcc Al (free-electronlike) metal $K_{\text{Al}} = 1.6 \times 10^{-3}$ is by a factor of ~3 larger, owing to the higher electrical conductivity (larger electronic DOS at ε_{F}), than the $\text{Al}_{0.5}\text{TiZrPdCuNi}$ HEA and MG samples.

The theoretical $I = \frac{5}{2}$ quadrupole-perturbed NMR spectrum of a structurally and chemically disordered nonmagnetic metallic alloy can be calculated via the steps used before to reproduce the ^{27}Al spectra of quasicrystals (translationally nonperiodic, long-range-ordered structures with crystallographically forbidden symmetries) [14–16] and complex metallic alloys (giant-unit-cell intermetallics with inherent structural and chemical disorder) [17]. By considering that each resonant nucleus in principle resides in a different local chemical environment, the NMR frequency of the $m \leftrightarrow m-1$ spin transition of the ith nucleus is [18]

$$\nu_i(m) - \nu_0 = \nu_{\text{quad},i}^{(1)}(m) + \nu_{\text{quad},i}^{(2)}\left(\tfrac{1}{2}\right) + \nu_{\text{mag},i}, \qquad (1)$$

where $\nu_0 = \gamma_n B_0/2\pi$ is the Zeeman frequency in an external magnetic field B_0, and γ_n is the nuclear gyromagnetic ratio. The terms $\nu_{\text{quad},i}^{(1)}(m)$ and $\nu_{\text{quad},i}^{(2)}\left(\tfrac{1}{2}\right)$ are the first- and second-order quadrupole shifts, respectively, where the first-order shift affects all $m \leftrightarrow m-1$ spin transitions except the central one $\left(\tfrac{1}{2} \leftrightarrow -\tfrac{1}{2}\right)$, whereas the second-order shift is consequently important only for the central transition. Their explicit forms are

$$\nu_{\text{quad},i}^{(1)}(m) = -\frac{\nu_{Q,i}}{2}\left(m - \frac{1}{2}\right)(3\cos^2\theta_i - 1 + \eta_i\sin^2\theta_i\cos2\phi_i), \qquad (2)$$

and

$$\nu_{\text{quad},i}^{(2)}\left(\frac{1}{2}\right) = \frac{\nu_{Q,i}^2}{12\nu_0}\left[6\sin^2\theta_i(1 - 9\cos^2\theta_i) - 4\eta_i\cos2\phi_i\sin^2\theta_i(9\cos^2\theta_i + 1) + \eta_i^2\left(-\frac{16}{3} + 8\cos^2\theta_i + 6\cos^22\phi_i\sin^4\theta_i\right)\right]. \qquad (3)$$

Here $\nu_{Q,i} = 3eV_{ZZ}^{(i)}Q/20h$ is the quadrupole coupling constant, determined by the largest principal value $V_{ZZ}^{(i)}$ of the EFG tensor at the ith lattice site, Q is the nuclear electric quadrupole moment, and h is Planck's constant. Here, $V_{ZZ}^{(i)}$ can be written as

$$V_{ZZ}^{(i)} = V_{ZZ,i}^{\text{ion}}\left[1 - \gamma_\infty^{(i)}\right] + V_{ZZ,i}^{el}, \qquad (4)$$

where the first term describes the ionic contribution to the EFG, with $1 - \gamma_\infty^{(i)}$ denoting the Sternheimer antishielding factor due to polarization of the core electronic shells, whereas the second term describes the contribution from the conduction electrons. Here, θ_i and ϕ_i are polar and azimuthal angles, describing the orientation of the EFG principal-axes system (PAS), denoted as (X, Y, Z) relative to the laboratory

frame (x, y, z), where the external magnetic field is applied along the z direction. The quantity $\eta_i = [V_{XX}^{(i)} - V_{YY}^{(i)}]/V_{ZZ}^{(i)}$ is the quadrupole asymmetry parameter, with the EFG-tensor principal values arranged as $|V_{XX}^{(i)}| \leqslant |V_{YY}^{(i)}| \leqslant |V_{ZZ}^{(i)}|$.

The magnetic shift $\nu_{\text{mag},i}$ originates from the local magnetic field produced at the resonant nuclei by the magnetization of the conduction electrons induced in B_0. It can be written as

$$\nu_{\text{mag},i} = \frac{\gamma_n}{2\pi}\left[K_i + \frac{K_{Z,i}}{2}(3\cos^2\theta_i' - 1 + \varepsilon_i\sin^2\theta_i'\cos2\phi_i')\right]B_0, \qquad (5)$$

where the isotropic Knight shift K_i originates from the Fermi contact interaction of the nucleus with the s-type conduction

electrons, whereas the traceless anisotropic Knight shift tensor with the largest principal value $K_{Z,i}$ and the asymmetry parameter $\varepsilon_i = (K_{X,i} - K_{Y,i})/K_{Z,i}$ originate from the dipolar coupling between the nucleus and the spins of the conduction electrons. The orientation of the PAS of the Knight-shift tensor relative to the external magnetic field is described by the angles θ_i' and ϕ_i'. The anisotropic Knight shift produces inhomogeneous broadening of the spectrum, whereas the isotropic Knight shift produces a shift of its center of gravity.

The distribution of the site-specific parameters $V_{ZZ}^{(i)}$, η_i, K_i, K_Z^i, ε_i, θ_i, ϕ_i, θ_i', and ϕ_i' introduces inhomogeneous broadening of the NMR spectrum, whereas their average values shift the spectrum on the frequency axis. Since in the HEAs and MGs there exists a large manifold of different local chemical environments, we assume that the parameters are distributed by a continuous distribution function $G(V_{ZZ}, \eta, K, K_Z, \varepsilon, \theta, \phi, \theta', \phi')$. The frequency spectrum corresponding to the $m \leftrightarrow m-1$ transition of a single-grain sample is then obtained as

$$F_m(\nu) = \int \delta[\nu - \nu(m)] G(V_{ZZ}, \eta, K, K_Z, \varepsilon, \theta, \phi, \theta', \phi') d\tau, \tag{6}$$

where $d\tau$ refers to the differential of all nine parameters in the distribution G. For a crystalline powder or a polygrain bulk sample with random orientation of the grains, a powder average must be performed as well. The final spectrum is obtained by summing up the spectra $F_m(\nu)$ of all spin transitions, each one weighted by the respective amplitude $\beta_m = I(I+1) - m(m-1)$:

$$I(\nu) = \sum_{m=5/2}^{-3/2} \beta_m F_m(\nu). \tag{7}$$

Regarding the multiparameter distribution function G pertinent to the investigated HEA and MG samples, the experimental spectra of Fig. 1 indicate that the first-order quadrupolar broadening is by far dominant over the broadening induced by the anisotropic Knight shift, so that the latter can be neglected. In addition, the smallness of the isotropic Knight shift allows replacing K_i by an average value over all sites, $\langle K_i \rangle = K$, so that Eq. (1) becomes

$$\nu_i(m) - \nu_0 = \frac{\gamma_n}{2\pi} K B_0 + \nu_{\text{quad},i}^{(1)}(m) + \nu_{\text{quad},i}^{(2)}\left(\frac{1}{2}\right). \tag{8}$$

The distribution function $G(V_{ZZ}, \eta, \theta, \phi)$ then depends only on the four parameters that characterize the magnitude and orientation of the EFG tensors. Further simplification comes from the assumption that the distribution of the EFG-tensor orientations is independent of the distribution of the eigenvalues, so that $G(V_{ZZ}, \eta, \theta, \phi) = f(V_{ZZ}, \eta) h(\theta, \phi)$. For the amorphous MG and the polygrain HEA samples, it is reasonable to assume that the EFG-tensor orientations are distributed uniformly on a sphere, in which case the integration over the distribution $h(\theta, \phi)$ can be replaced by a powder average $(1/4\pi) d\Omega = (1/4\pi) \sin\theta d\theta d\phi$, with $0 \leqslant \theta \leqslant \pi$ and $0 \leqslant \phi \leqslant 2\pi$. By considering that the distribution of the EFG tensor eigenvalues is described by a function $f(V_{ZZ}, \eta)$, whose analytical form will be presented in the following, Eq. (6)

becomes

$$F_m(\nu) = \int_0^{2\pi} d\phi \int_0^\pi \sin\theta d\theta \int_0^1 d\eta \int_{-\infty}^\infty dV_{ZZ}$$
$$\times \delta[\nu - \nu(m)] f(V_{ZZ}, \eta), \tag{9}$$

with $\nu(m)$ now given by Eq. (8) (dropping the subscript i).

The theoretical distribution $f(V_{ZZ}, \eta)$ for a random distribution of electric charges was derived by Czjzek *et al.* [19] and reviewed by Le Caër and Brand [20]. A general functional form was derived, known as the Gaussian isotropic model (GIM) [19,20], which assumes that all five EFG-tensor elements are Gaussian independent variables. The derivation of $f(V_{ZZ}, \eta)$ is not restricted to a point-charge model and is applicable to amorphous solids that are isotropic on average [19] and to cubic lattices with a large number of defects [21], hence being suitable to both MGs and cubic HEAs. The GIM distribution function is given by

$$f(V_{ZZ}, \eta) = \frac{V_{ZZ}^4 \eta}{\sqrt{2\pi} \sigma^5} \left(1 - \frac{\eta^2}{9}\right) \exp\left[-\frac{V_{ZZ}^2}{2\sigma^2}\left(1 + \frac{\eta^2}{3}\right)\right], \tag{10}$$

which contains only one fit parameter σ that determines the width of the distribution. The joint (bivariate) distribution function $f(V_{ZZ}, \eta)$ is hard to visualize directly, but it is straightforward to calculate analytically and then visualize the two marginal distributions:

$$f_a(\eta) = \int_{-\infty}^\infty dV_{ZZ} \, f(V_{ZZ}, \eta) = \frac{3\eta(1 - \eta^2/9)}{(1 + \eta^2/3)^{5/2}}, \tag{11a}$$

and

$$\begin{aligned} f_e(V_{ZZ}) &= \int_0^1 d\eta \, f(V_{ZZ}, \eta) \\ &= \frac{1}{\sigma}\sqrt{\frac{2}{\pi}}\left[\left(\frac{3V_{ZZ}^2}{2\sigma^2} - 1\right)\exp\left(-\frac{V_{ZZ}^2}{2\sigma^2}\right) \right. \\ &\left. + \left(1 - \frac{4V_{ZZ}^2}{3\sigma^2}\right)\exp\left(-\frac{2V_{ZZ}^2}{3\sigma^2}\right)\right]. \end{aligned} \tag{11b}$$

Theoretical fits of the experimental lineshapes using Eqs. (7)–(10) are shown in the right column of Fig. 1. The fits are excellent, reproducing accurately both the shape of the spectra and their field-dependence [best seen on the central lines in Figs. 2(a) and 2(b)] by adjusting a single fit parameter, the width σ of the GIM distribution (and changing the Larmor frequency ν_0). For the HEA sample, the fit parameter value is $\sigma_{\text{HEA}} = 90 \pm 5$ kHz, while for the MG sample, it is significantly larger, $\sigma_{\text{MG}} = 157 \pm 3$ kHz. The natural (homogeneous) widths of the spectra were taken as $\sigma_{\text{HEA}}^{\text{hom}} = 11$ kHz and $\sigma_{\text{MG}}^{\text{hom}} = 21$ kHz and convoluted with the GIM distribution.

The graphs of the resulting marginal distributions $f_e(V_{ZZ})$ and $f_a(\eta)$ are displayed in Fig. 3, where the following features are evident:

(a) The V_{ZZ} distributions of both samples, $f_e^{\text{HEA}}(V_{ZZ})$ and $f_e^{\text{MG}}(V_{ZZ})$, shown in Fig. 3(a) exhibit a hole around $V_{ZZ} = 0$ with zero probability for $V_{ZZ} = 0$ and very small probabilities for small values of V_{ZZ}. The physical significance of this result is the vanishingly small probability for highly symmetric local atomic configurations in a strongly disordered solid.
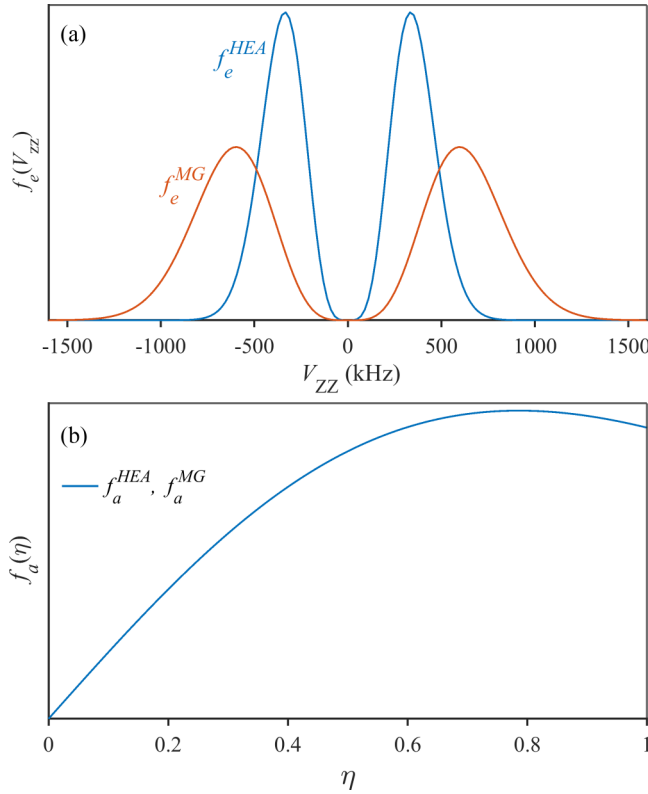
FIG. 3. (a) Marginal distributions $f_e^{\text{HEA}}(V_{ZZ})$ and $f_e^{\text{MG}}(V_{ZZ})$, describing the distribution of the V_{ZZ} electric-field-gradient (EFG)-tensor element in the high-entropy alloy (HEA) and metallic glass (MG) samples, respectively. The quantity V_{ZZ} on the graph (in units of kilohertz) is not the true V_{ZZ} (in units of volts per square meter) as defined by Eq. (4), but a renormalized quantity $3eV_{ZZ}Q/40h$. (b) Marginal distributions $f_a^{\text{HEA}}(\eta)$ and $f_a^{\text{MG}}(\eta)$, describing the distribution of the asymmetry parameter η of the EFG tensor in the HEA and MG samples (the two distributions are identical).

(b) The $f_e^{\text{MG}}(V_{ZZ})$ distribution of the MG sample is roughly by a factor 2 broader than $f_e^{\text{HEA}}(V_{ZZ})$ of the HEA sample, revealing stronger topological and chemical disorder in the amorphous MG state, as compared with the crystalline HEA state.

(c) The η distributions $f_a^{\text{HEA}}(\eta)$ and $f_a^{\text{MG}}(\eta)$ shown in Fig. 3(b) are equal, exhibiting zero probability at $\eta = 0$, reflecting the fact that the symmetric case $\eta = 0$, or equivalently $V_{XX} = V_{YY}$, has zero probability in both the HEA and the MG samples.

It is instructive to compare the $I = \frac{5}{2}$ NMR lineshape of the HEA and MG states with the respective lineshape of a powder specimen of a perfectly ordered, translationally periodic crystal, having a single crystallographic site for the resonant nucleus in the unit cell. It that case, there is only one EFG tensor (single V_{ZZ} and η values) instead of the $f(V_{ZZ}, \eta)$ distribution, whose PAS is distributed isotropically on a sphere. In Fig. 4, we compare the theoretical spectra of the HEA and MG samples [the fits shown in Figs. 1(e) and 1(g), respectively] with the powder spectra of the ordered crystal for two values of the asymmetry parameter, $\eta = 0$ and 1. The differences are best seen in the satellite part of the spectra, which for the HEA and MG show a featureless Gaussian shape, while the ordered
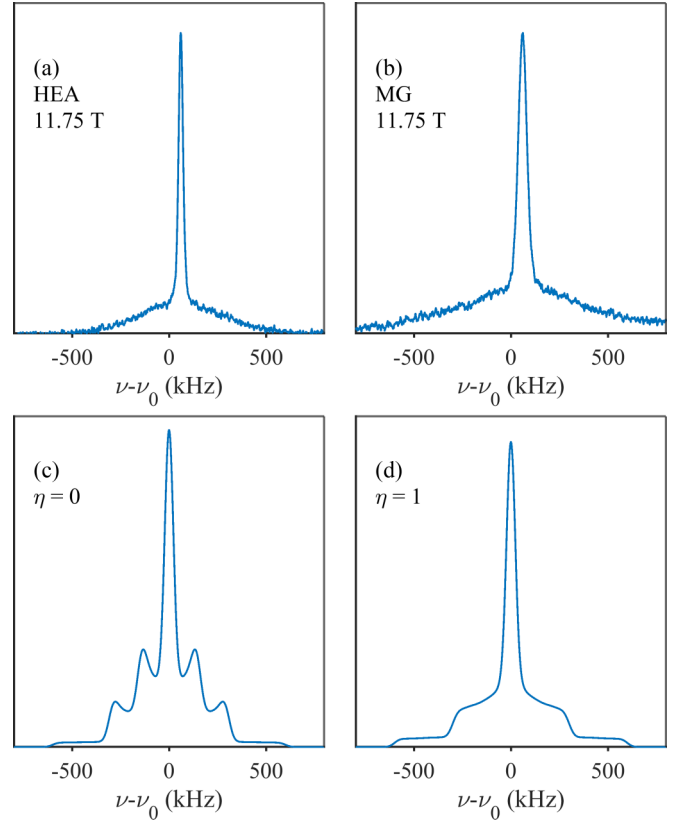

FIG. 4. Comparison of the theoretical $I = \frac{5}{2}$ quadrupole-perturbed nuclear magnetic resonance (NMR) spectra of the high-entropy alloy (HEA) and metallic glass (MG) samples with the powder spectrum of a perfectly ordered, translationally periodic crystal, having a single crystallographic site for the resonant nucleus in the unit cell. (a) HEA spectrum [the spectrum from Fig. 1(e)], (b) MG spectrum [the spectrum from Fig. 1(g)], (c) powder spectrum of the ordered crystal for $\eta = 0$, and (d) powder spectrum of the ordered crystal for $\eta = 1$. The spectra in (c) and (d) were scaled to match approximately the spectra in (a) and (b).

crystal shows substructure and sharp features originating from the shapes and intensities of the individual $\pm\frac{1}{2} \leftrightarrow \pm\frac{3}{2}$ and $\pm\frac{3}{2} \leftrightarrow \pm\frac{5}{2}$ transitions.

The isotropic Knight shift generally depends on temperature, where the temperature-dependence originates from the Fermi-Dirac function and the fact that the Fermi energy (more precisely, the chemical potential μ) itself depends on temperature [15,22]. Denoting by ε_F the Fermi energy at $T = 0$, the temperature-dependent Knight shift is [15]

$$K(T) = K^0 \left(1 + \left(\frac{\pi^2 k_B^2}{6}\right) \left\{ \left[\frac{g''(\varepsilon_F)}{g(\varepsilon_F)}\right] - \left[\frac{g'(\varepsilon_F)}{g(\varepsilon_F)}\right]^2 \right\} T^2 \right), \tag{12}$$

where $g'(\varepsilon)$ and $g''(\varepsilon)$ are the first and second derivatives of the electronic DOS $g(\varepsilon)$ with respect to energy. The temperature-independent Knight shift K^0 is

$$K^0 = \left(\frac{\mu_0}{3}\right) \hbar^2 \gamma_e^2 \langle |u_k^2(0)| \rangle_{\varepsilon_F} g(\varepsilon_F), \tag{13}$$

where γ_e is the electronic gyromagnetic ratio, μ_0 is the permeability of vacuum, and $\langle |u_k^2(0)| \rangle$ is the density of the (s-type)
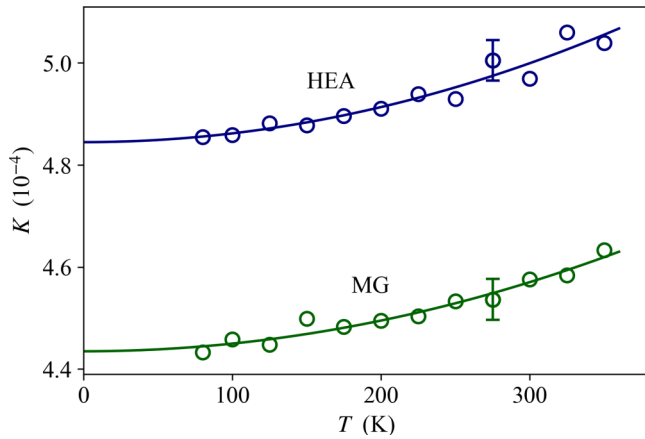
FIG. 5. Temperature-dependent Knight shift of the high-entropy alloy (HEA) and metallic glass (MG) samples measured in $B_0 = 8.926$ T. Solid curves are fits $K = K^0 + \alpha T^2$, and the fit parameters are given in the text.

conduction-electron wave function at the nucleus, averaged over the Fermi surface. In free-electronlike metals, the DOS does not change with energy significantly within the Fermi level region, so that the derivatives $g'(\varepsilon_F)$ and $g''(\varepsilon_F)$ are small, and the Knight shift is essentially temperature independent. For a significant variation of $g(\varepsilon)$ within the Fermi level region, a T^2 dependence of the Knight shift is observed.

The temperature-dependent Knight shift of the HEA and MG samples was extracted from the total frequency shift $\Delta \nu$ of the respective central lines, which was measured in $B_0 = 8.926$ T between 80 and 350 K. The second-order quadrupolar shift determined at 200 K was subtracted from the total shift by assuming that it is temperature independent (here, we neglect the possible tiny strengthening of the quadrupolar interaction upon cooling due to the EFG increase by thermal contraction of the material). The $K(T)$ data are displayed in Fig. 5, together with the fits $K = K^0 + \alpha T^2$. The fit parameters are $K_{HEA}^0 = 4.85 \times 10^{-4}$ and $\alpha_{HEA} = 1.72 \times 10^{-10}$ K^{-2} for the HEA sample and $K_{MG}^0 = 4.43 \times 10^{-4}$ and $\alpha_{MG} = 1.51 \times 10^{-10}$ K^{-2} for the MG sample.

IV. DISCUSSION AND CONCLUSIONS

The presented analysis of the ^{27}Al NMR lineshape confirms that the crystalline HEA and the amorphous MG states of the Al$_{0.5}$TiZrPdCuNi alloy both contain an enormous, continuous manifold of local chemical environments due to the immense topological and chemical disorder. The distribution of magnitudes of the EFG-tensor eigenvalues is well described by the GIM, compatible with statistical mixing of the chemical elements. This distribution is about twice broader in the MG state as compared with the HEA state, reflecting the existence of a (distorted) crystal lattice in the latter and its complete absence in the former. The distribution of the EFG-tensor PAS orientations is well approximated by an isotropic distribution on a sphere for both structural modifications. The HEA and the MG states of the Al$_{0.5}$TiZrPdCuNi alloy consequently classify among the extremely disordered solids at the level of local, near-neighbor atomic environments. Regarding the local electronic structure at the ^{27}Al nuclei, the

T^2 dependence of the Knight shift indicates that the DOS derivatives $g'(\varepsilon_F)$ and $g''(\varepsilon_F)$ are significant for both structural modifications, so that the HEA and the MG states share a common property of a rapidly changing DOS with energy within the Fermi level region. This is quite different from free-electronlike metals and alloys but agrees with the results of electrical resistivity and thermoelectric power of the same HEA and MG samples [6], where the temperature dependence was shown to originate from the strong variation of the spectral conductivity (directly related to the electronic DOS) with energy within the Fermi level region. The temperature-independent part K^0 of the Knight shift allows estimating the ratio of the HEA and the MG electronic DOS at ε_F, yielding $K_{HEA}^0 / K_{MG}^0 \approx g_{HEA}(\varepsilon_F) / g_{MG}(\varepsilon_F) = 1.1$ (where we have used the approximation that $\langle |u_{\vec{k}}^2(0)| \rangle$ of the HEA and the MG states is the same). This value is in good agreement with the values determined independently from the linear coefficient of the specific heat $g_{HEA}(\varepsilon_F) / g_{MG}(\varepsilon_F) = 1.27$ and the Pauli spin susceptibilities $g_{HEA}(\varepsilon_F) / g_{MG}(\varepsilon_F) \approx 1.1$ [6]. The local electronic structure of the HEA and the MG states is hence not much different, despite the existence of a crystal lattice in the former and its absence in the latter.

The NMR-determined parameters of the HEA state [the V_{ZZ} distribution $f_e^{HEA}(V_{ZZ})$ and the η distribution $f_a^{HEA}(\eta)$ shown in Fig. 3 and the Knight shift K_{HEA} shown in Fig. 5] are average quantities over the two structural phases that appear in the HEA sample, the bcc that occupies $\sim 70\%$ of the volume of the sample and the Heusler alloy, occupying $\sim 30\%$ of the volume. As already discussed, the two phases are structurally closely related, and the employed chemical elements are highly soluble in both phases, so that the entire HEA lattice can be loosely viewed as a single bcc structure, with a larger part of it chemically disordered in a statistical manner and a smaller part partially ordered but still having significant substitutional disorder. In this case, it is reasonable to assume that the GIM of the EFG distribution is applicable to both phases. To study each of the two phases independently is unfeasible because there is no known synthesis route to produce single-phase materials within the Al$_{0.5}$TiZrPdCuNi system that would possess the same chemical disorder as the investigated two-phase sample.

To conclude, the presented ^{27}Al NMR study of the Al$_{0.5}$TiZrPdCuNi alloy has allowed an insight into the local structural and electronic properties of a HEA material, in relation to its MG counterpart. No other local study of a HEA material by any local spectroscopic technique can be found in literature at the time of writing. Another important result of this paper is a theoretical calculation of the quadrupole-perturbed spin $\frac{5}{2}$ NMR spectrum of the HEA and MG states, to serve as a reference for future NMR studies of Al-containing HEAs and MGs. Since the aluminum element is frequently employed as one of the components in multicomponent mixtures, such HEAs and MGs are numerous.

[1] J. W. Yeh, S. K. Chen, S. J. Lin, J. Y. Gan, T. S. Chin, T. T. Shun, C. H. Tsau, and S. Y. Chang, Nanostructured high-entropy alloys with multiple principal elements: Novel alloy design concepts and outcome, Adv. Eng. Mater. **6**, 299 (2004).

[2] B. Cantor, I. T. H. Chang, P. Knight, and A. J. B. Vincent, Microstructural development in equiatomic multicomponent alloys, Mater. Sci. Eng. A **375** 213 (2004).

[3] Y. Zhang, T. T. Zuo, Z. Tang, M. C. Gao, K. A. Dahmen, P. K. Liaw, and Z. P. Lu, Microstructures and properties of high-entropy alloys, Prog. Mat. Sci. **61**, 1 (2014), and references therein.

[4] *High-Entropy Alloys*, 2nd ed., edited by B. S. Murthy, J.-W. Yeh, S. Ranganathan, and P. P. Bhattacharjee (Elsevier, Amsterdam, 2019).

[5] *High-Entropy Alloys: Fundamentals and Applications*, edited by M. C. Gao, J.-W. Yeh, P. K. Liaw, and Y. Zhang (Springer International Publishing Switzerland, Cham, 2016).

[6] M. Wencka, M. Krnel, A. Jelen, S. Vrtnik, J. Luzar, P. Koželj, D. Gačnik, A. Meden, Q. Hu, C. Wang, S. Guo, and J. Dolinšek, Electronic transport properties of the $Al_{0.5}TiZrPdCuNi$ alloy in the high-entropy alloy and metallic glass forms, Sci. Rep. **12**, 2271 (2022).

[7] A. Takeuchi, J. Wang, N. Chen, W. Zhang, Y. Yokoyama, K. Yubuta, and S. Zhu, $Al_{0.5}TiZrPdCuNi$ high-entropy (H-E) alloy developed through $Ti_{20}Zr_{20}Pd_{20}Cu_{20}Ni_{20}$ H-E glassy alloy comprising inter-transition metals, Mater. Trans. **54**, 776 (2013).

[8] T. Nagase, A. Takeuchi, K. Amiya, and T. Egami, Solid state amorphization of metastable $Al_{0.5}TiZrPdCuNi$ high entropy alloy investigated by high voltage electron microscopy, Mater. Chem. Phys. **210**, 291 (2018).

[9] A. Takeuchi and A. Inoue, Classification of bulk metallic glasses by atomic size difference, heat of mixing and period of constituent element and its application to characterization of the main alloying element, Mater. Trans. **46**, 2817 (2005).

[10] L. Ma, L. Wang, T. Zhang, and A. Inoue, Bulk glass formation of Ti-Zr-Hf-Cu-*M* (*M* = Fe, Co, Ni) alloys, Mater. Trans. **43**, 277 (2002).

[11] K. Zhao, X. X. Xia, H. Y. Bai, D. Q. Zhao, and W. H. Wang, Room temperature homogeneous flow in a bulk metallic glass with low glass transition temperature, Appl. Phys. Lett. **98**, 141913 (2011).

[12] A. Takeuchi, N. Chen, T. Wada, Y. Yokoyama, H. Kato, A. Inoue, and J. W. Yeh, $Pd_{20}Pt_{20}Cu_{20}Ni_{20}P_{20}$ high-entropy alloy as a bulk metallic glass in the centimeter, Intermetallics **19**, 1546 (2011).

[13] X. Q. Gao, K. Zhao, H. B. Ke, D. W. Ding, W. H. Wang, and H. Y. Bai, High mixing entropy bulk metallic glasses, J. Non-Cryst. Solids **357**, 3557 (2011).

[14] A. Shastri, F. Borsa, D. R. Torgeson, J. E. Shield, and A. I. Goldman, NMR and NQR study of the electronic and structural properties of Al-Cu-Fe and Al-Cu-Ru quasicrystals, Phys. Rev. B **50**, 15651 (1994).

[15] E. A. Hill, T. C. Chang, Y. Wu, S. J. Poon, F. S. Pierce, and Z. M. Stadnik, Temperature-dependent NMR features of the $Al_{65}Cu_{20}Ru_{15}$ icosahedral alloy, Phys. Rev. B **49**, 8615 (1994).

[16] P. Jeglič and J. Dolinšek, NMR features of a decagonal $Al_{72.6}Ni_{10.5}Co_{16.9}$ quasicrystal, Phys. Rev. B **71**, 014204 (2005).

[17] P. Jeglič, M. Komelj, M. Klanjšek, U. Tkalec, S. Vrtnik, M. Feuerbacher, and J. Dolinšek, Orientation-dependent NMR study of the giant-unit-cell intermetallics β-Al_3Mg_2, Bergman-phase $Mg_{32}(Al, Zn)_{49}$, and $\xi' - Al_{74}Pd_{22}Mn_4$, Phys. Rev. B **75**, 014202 (2007).

[18] J. Winter, *Magnetic Resonance in Metals* (Clarendon Press, Oxford, 1971), Chaps. II, IV, and V.

[19] G. Czjzek, J. Fink, F. Götz, H. Schmidt, J. M. D. Coey, J.-P. Rebouillat, and A. Liénard, Atomic coordination and the distribution of electric field gradients in amorphous solids, Phys. Rev. B **23**, 2513 (1981).

[20] G. Le Caër and R. A. Brand, General models for the distributions of electric field gradients in disordered solids, J. Phys.: Condens. Matter **10**, 10715 (1998).

[21] H. J. Stöckmann, Electric field gradients resulting from randomly distributed unscreened point charges, J. Magn. Reson. **44**, 145 (1981).

[22] Ref. [18], pp. 114–117.